

# Effect of nanostructures on the exothermic reaction and ignition of Al/CuOx based energetic materials

Yang Yang · Daguo Xu · Kaili Zhang

Received: 22 May 2011 / Accepted: 25 August 2011 / Published online: 8 September 2011  
© Springer Science+Business Media, LLC 2011

**Abstract** Al/CuOx based micro- and nanoenergetic materials (EMs) have been made by the thermal oxidation of Cu thin films deposited onto silicon substrates followed by Al integration through thermal evaporation. The micro- and nano-EMs are then characterized by scanning electron microscopy, energy dispersive X-ray analysis, X-ray diffraction, differential thermal analysis, and differential scanning calorimetry. By comparing the thermite reactions and ignition properties of Al with micro-CuOx and Al with nano-CuOx, we show experimentally that one-dimensional nanostructures (CuO nanowires) and nano-Al affect greatly the exothermic behaviors and ignition properties of the Al/CuOx based EMs. The higher surface energy associated with the CuO nanowires and the deposited nano-Al is believed to be a possible factor contributing to the enhanced exothermic reactions that occur below the melting point of Al and the smaller ignition delay and lower ignition energy.

## Introduction

Energetic materials (EMs) are a class of reactive materials that include propellants, explosives, and pyrotechnics. EMs have found numerous civilian and defense applications [1, 2]. In recent times, nanoenergetic materials (nEMs) have received steadily growing interest due to their improved performances in terms of energy release, ignition, and other thermal properties compared to their bulk or

microcounterparts caused by the much larger specific surface areas of the reactants [3–20]. Various ways have been used to realize nEMs, where physical mixing (by ultrasonic, electrostatic, etc.) of nanoparticles of fuel (mainly Al) and oxidizer is the most employed approach [4, 6–11, 13–18]. Physical mixing is simple and convenient, but it presents some limitations such as a non-homogeneous distribution of oxidizer and fuel, and especially, a poor compatibility with a microsystem. A nano-Al/CuO based nEM has been made by integrating nano-Al with CuO nanowires grown from a Cu film deposited onto silicon [21]. This approach has the advantages of enhanced contact, reduced impurities and Al oxidation, and especially, easier integration into the microsystem because the nEM is fabricated onto silicon, a basic material for microelectronics and microsystems. Recently, a functional electro-explosive device, a nanoinitiator was developed by integrating the Al/CuO based nEM with a Au/Pt/Cr thin film microheater realized onto a substrate [22].

Exothermic reaction and ignition are important properties of EMs. Significantly enhanced exothermic reactions have been observed in nEMs based on physical mixing of fuel/oxidizer nanoparticles compared to those for EMs based on physical mixing of fuel/oxidizer microparticles [7, 11, 14]. Besides the physical mixing of nanoparticles of fuel and oxidizer, the self-assembly of the fuel (mainly Al) with one-dimensional (1D nanowires/rods) oxidizer is another promising approach that has been widely used to realize nEMs [5, 12, 20, 21]. Ignition has been achieved for Al and Fe<sub>2</sub>O<sub>3</sub> nanowires based nEM in [5] and the ignition temperature was found to be below the melting point of Al. In Ref. [12], the combustion behaviors (velocity, pressure, etc.) of Al and CuO nanorods based nEMs were studied. References [21, 22] proved the feasibility of realizing Al/CuO based nEMs by integrating Al with CuO nanowires

Y. Yang · D. Xu · K. Zhang (✉)  
Department of Mechanical and Biomedical Engineering,  
City University of Hong Kong, 83 Tat Chee Avenue,  
Kowloon, Hong Kong, China  
e-mail: kaizhang@cityu.edu.hk; kaili\_zhang@hotmail.com

grown from a Cu film deposited onto silicon. However, no detailed studies on the exothermic reactions and ignition properties of the Al/CuO based EMs were investigated. Furthermore, there are very few investigations in the literature to compare the exothermic reactions and ignition properties of the microscale and nanoscale EMs that are based on the self-assembly of the fuels with 1D nano-oxidizers.

In this study, scanning electron microscopy (SEM), energy dispersive X-ray analysis (EDX), X-ray diffraction (XRD), differential thermal analysis (DTA), and differential scanning calorimetry (DSC) are used to investigate the exothermic reactions of the Al/CuOx based EMs that are synthesized by integrating Al with 1D CuOx nanostructures (CuO nanowires) and also with micro-CuOx. The structures and components of Al/CuOx based materials in various temperature environments are carefully studied, which are important for manufacturing applications. Also, the authors showed experimentally that the CuO nanowires and nano-Al can enhance the exothermic reactions and ignition properties of the Al/CuOx based EMs. This is important for engineers and scientists to control the reactivity and ignition of energetic materials.

## Experiments

The experimental process starts with a 500  $\mu\text{m}$  thick double polished 4-inch (100 mm) p-type silicon substrate. The substrate is cleaned using acetone, a chromic sulfuric acid mixture, thoroughly rinsed by de-ionized (DI) water and blow-dried by nitrogen. Then the substrate is placed into an oven at 200  $^{\circ}\text{C}$  for 20 min for further drying. A Ti film with a thickness of 30 nm is first deposited by thermal evaporation onto the silicon substrate to act as the adhesion layer between Cu and the substrate. A Cu film with a thickness of 50 nm is then deposited onto the Ti layer by thermal evaporation. The 50 nm Cu film serves as the electrical conducting layer for the subsequent electroplating. The thermal evaporation for Ti and Cu is performed under a vacuum level of  $5 \times 10^{-6}$  mbar and the substrate temperature is about 40  $^{\circ}\text{C}$  during the deposition. A Cu film with a thickness of 1  $\mu\text{m}$  is deposited by electroplating at 25  $^{\circ}\text{C}$ . The Cu electroplating is performed with a current density of 1 A/dm<sup>2</sup> under a continuous mode. The silicon substrate with the Cu film is cut into chips and they are cleaned for 25 s in a solution of 10 mL HCl (37%) and 120 mL DI water. After being rinsed with DI water and blow-dried by nitrogen, the chips are placed onto a clean silicon wafer that is put onto a quartz boat. The quartz boat is positioned into the center of a quartz tube (100 cm in length, 17 cm in diameter) that is mounted inside a horizontal tube furnace. The chips are then thermally oxidized

in the furnace in static air. After being held for the prescribed temperature and time, the furnace is cooled down naturally to room temperature. During the thermal oxidation, the Cu film is converted into CuO nanowires, CuO micro/nanoparticles, and/or a Cu<sub>2</sub>O film depending on the oxidation temperature. Finally, Al is deposited by thermal evaporation onto the silicon substrate with the CuO/Cu<sub>2</sub>O micro/nanostructures. Al is deposited under a vacuum level of  $5 \times 10^{-6}$  mbar and the substrate temperature is about 30  $^{\circ}\text{C}$  during the deposition. For comparison purpose, the deposited film thickness of Al is set at 1.12  $\mu\text{m}$  (on average across the sample) in the thermal evaporator for all the experiments. This Al thickness is 1.2 times larger than the stoichiometry thickness for the reactions between Al and CuO so as to achieve slightly fuel-rich mixtures (i.e., equivalence ratio 1.2). The slightly fuel-rich mixtures have been proven to have lower ignition time and higher combustion velocity compared to those for stoichiometric mixtures of Al and metal oxide based nEMs [7]. For determining the stoichiometric ratio, the mass of CuO is calculated based on the 1  $\mu\text{m}$  thick Cu thin film which is oxidized into CuO. Both the CuO nanowires and the CuO thin film layer underneath the nanowires are considered for determining the stoichiometry thickness.

The heat of reaction of the Al/CuOx EMs is determined by DTA and DSC. The DTA experiments are performed in the temperature range from 20 to 1000  $^{\circ}\text{C}$  with a heating rate of 15 K/min under a 99.995% Ar flow. The DSC experiments are carried out from 20 to 700  $^{\circ}\text{C}$  at a heating rate of 5 K/min under a 99.999% N<sub>2</sub> flow. Both for the DTA and DSC experiments, a second analysis is done on the same sample and in the same conditions in order to help the computation of the baseline correction. The Al/CuOx EMs are carefully scratched from the silicon substrate and collected for DTA and DSC experiments.

## Results

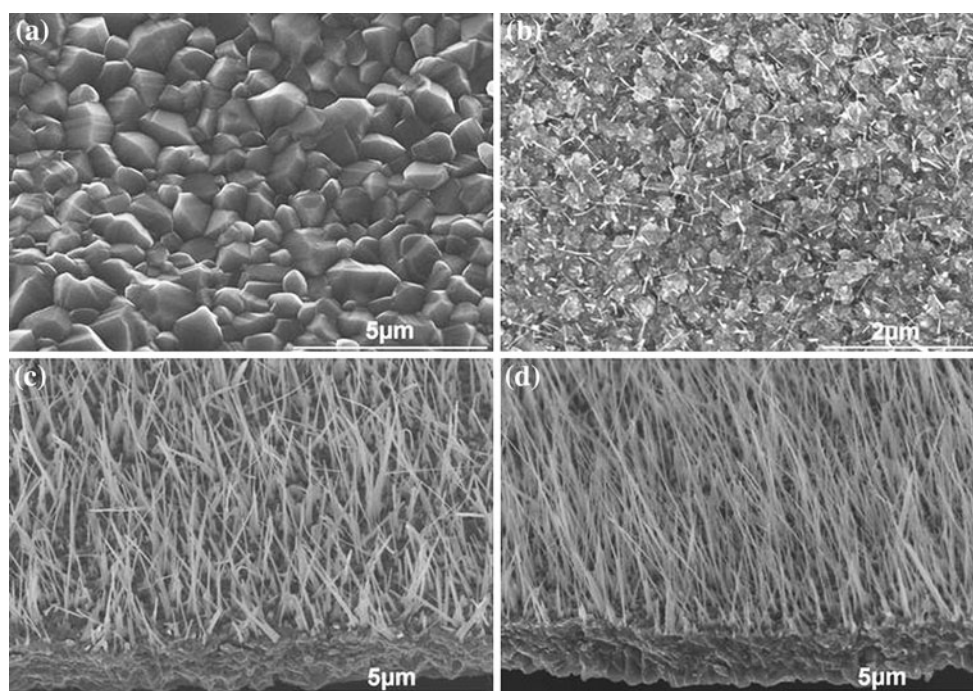
### SEM characterization

Figure 1a–d shows the SEM images of the oxidized 1  $\mu\text{m}$  thick Cu films in static air at 800  $^{\circ}\text{C}$  for 5 h, 360  $^{\circ}\text{C}$  for 5 h, 450  $^{\circ}\text{C}$  for 5 h, and 450  $^{\circ}\text{C}$  for 14 h, respectively. The oxidation process of Cu includes two steps:



When the Cu thin film is thermally oxidized in static air, Cu is first converted into Cu<sub>2</sub>O, and then CuO is formed slowly through a second step oxidation of Cu<sub>2</sub>O [23]. It is believed that the diffusion of O atoms controls the thermal oxidation process of the Cu film since O atoms are

**Fig. 1** SEM images of the oxidized 1  $\mu\text{m}$  thick Cu films in static air at: **a** 800  $^{\circ}\text{C}$  for 5 h, **b** 360  $^{\circ}\text{C}$ , 5 h, **c** 450  $^{\circ}\text{C}$ , 5 h, and **d** 450  $^{\circ}\text{C}$ , 14 h



significantly smaller than Cu atoms. The diffusion may occur on grain boundaries, sub-boundaries (dislocations), or within the lattice in the oxide layer depending on the temperature. When the Cu film is oxidized at low temperatures, the oxidation is dominated by grain boundary diffusion, which results in mainly micron size particles as shown in Fig. 1b where the Cu film is oxidized at 360  $^{\circ}\text{C}$  for 5 h. When the oxidation conditions are changed into 450  $^{\circ}\text{C}$  for 5 h, a large amount of oxide nanowires are formed on the film surface as shown in Fig. 1c. The oxidation should be dominated by diffusion through sub-boundaries (dislocations) and high density sub-boundaries will enhance the growth of the nanowires.

Figure 1d shows a SEM image of the Cu film after oxidation at 450  $^{\circ}\text{C}$  for 14 h. As compared to those in Fig. 1c, the nanowires become longer with a longer oxidation time. As shown in Eq. 1, when the Cu film is thermally oxidized in static air, Cu is first converted into  $\text{Cu}_2\text{O}$ . Since  $\text{Cu}_2\text{O}$  is not thermodynamically stable at 450  $^{\circ}\text{C}$ , CuO nanowires would start to grow due to the continuous supply of O from air and Cu from the copper film. During the growth process of the CuO nanowires,  $\text{Cu}_2\text{O}$  acts as the nucleation center. It has been confirmed that the presence of the  $\text{Cu}_2\text{O}$  seed phase is indispensable for the growth of CuO nanowires [24, 25]. In this experiment, the length of the nanowires is limited by the thickness of the deposited Cu film. After the entire film is oxidized into CuO (no  $\text{Cu}_2\text{O}$  presents any more), the

growth of the nanowires will stop even with further increasing the growth time.

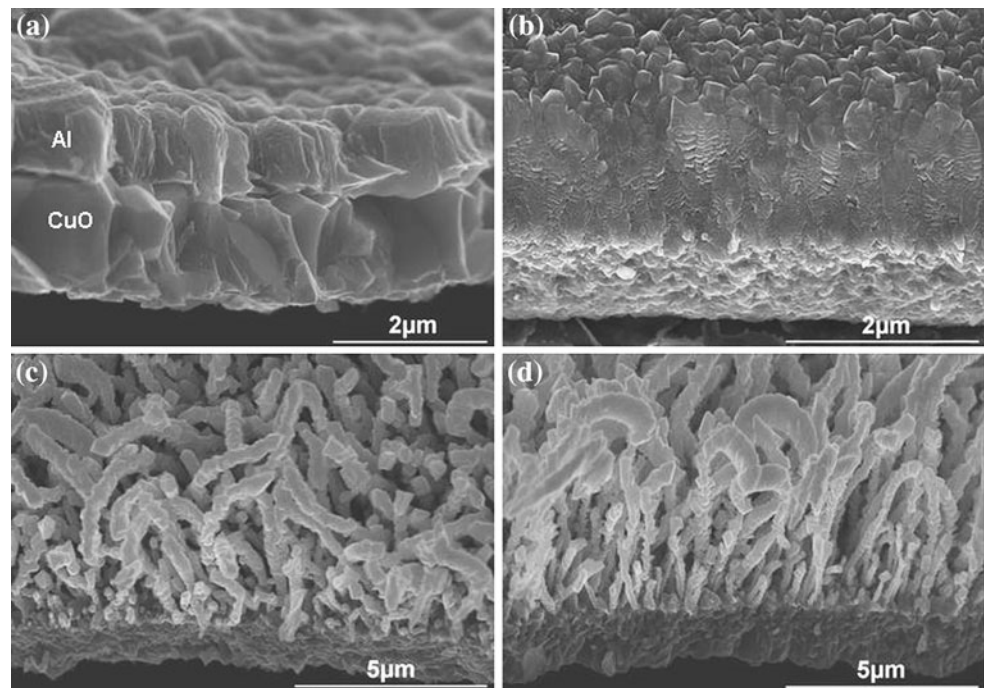
In accordance with Wagner's theory, at high-temperature a metal is oxidized through the lattice diffusion of the reacting atoms, ions or the transport of electrons through the dense scale [26]. Well crystallized microparticles are formed during oxidation of the Cu film at 800  $^{\circ}\text{C}$  as shown in Fig. 1a, which is caused by crystal growth. In the early heating stage, some nanowires are perhaps formed. But the high surface energy nanowires are not stable at high-temperature and they collapse to give microparticles.

Figure 2a–d shows the SEM images after Al deposition for the samples of Fig. 1a–d, respectively. For Fig. 2a and b, Al is deposited onto the thin film to form a layered structure. For Fig. 2c and d, it can be seen that Al is both uniformly integrated with the nanowires to form a core-shell nanostructure and also deposited onto the thin film beneath the nanowires to form a layered structure.

#### EDX characterization

Figure 3a–b shows the SEM image and EDX pattern of the front side of the Al/CuO nEMs after being scratched from the substrate, where the copper film is oxidized at 450  $^{\circ}\text{C}$  for 5 h. The main elements seen in the EDX spectrum are Al, Cu, and O. Figure 3c–d shows the SEM image and EDX pattern of the backside of the Al/CuO nEMs. The main elements seen in the EDX spectrum are Cu and O

**Fig. 2** SEM images of the oxidized 1  $\mu\text{m}$  thick Cu films in static air after Al deposition at: **a** 800  $^{\circ}\text{C}$  for 5 h, **b** 360  $^{\circ}\text{C}$ , 5 h, **c** 450  $^{\circ}\text{C}$ , 5 h, and **d** 450  $^{\circ}\text{C}$ , 14 h



since Al cannot be deposited on the backside. No Ti element is found from the scratched sample although 30-nm thick Ti is deposited onto the silicon substrate to act as the adhesion layer between Cu and the substrate. The main reason is that no much force is needed for the scratch because the adhesion between the oxidized copper film and the substrate is weak [27]. Therefore, the 30-nm thick Ti layer between the copper film and substrate will not be scratched away since the adhesion between Ti and silicon is very strong. Consequently, Ti can be considered not participating in the thermite reactions of the Al/CuO EMs. Figure 4 shows the SEM image and the element chemical map of the Al/CuO nEM, where the copper film is oxidized at 450  $^{\circ}\text{C}$  for 5 h.

#### XRD characterization

The as-prepared EMs are characterized by XRD as shown in Fig. 5a–d. After the 1  $\mu\text{m}$  thick Cu film is heated in static air at 800  $^{\circ}\text{C}$  for 5 h, the entire film is oxidized into CuO as can be seen in Fig. 5a, where the diffraction lines of Si is from the silicon substrate.  $\text{Cu}_2\text{O}$ , CuO, and Al diffraction lines can be seen in the XRD pattern in Fig. 5b, where the Cu film is oxidized at 360  $^{\circ}\text{C}$  for 5 h. It is shown in Fig. 5b that only a small part of the film is converted into CuO due to the slow conversion rate from  $\text{Cu}_2\text{O}$  to CuO at the low temperature of 360  $^{\circ}\text{C}$ . When the Cu film is heated at a higher temperature of 450  $^{\circ}\text{C}$  for 5 h, most of the Cu

film is converted into CuO as shown in Fig. 5c. If the oxidation time is increased from 5 to 14 h with the same oxidation temperature of 450  $^{\circ}\text{C}$ , the entire Cu film is oxidized into pure CuO as indicated in Fig. 5d. There are no peaks for metallic Cu in all the XRD patterns in Fig. 5a–d, indicating that no significant reaction between Al and  $\text{CuO}/\text{Cu}_2\text{O}$  occurs during the Al deposition due to the low silicon substrate temperature in the thermal evaporator.

#### DTA and DSC characterizations

There are two thermite reactions involved in the Al/CuOx based EMs as presented in Table 1 [28]. The adiabatic temperatures of the thermite reactions for Al/CuO and Al/ $\text{Cu}_2\text{O}$  are more or less same. However, the heat of reaction of Al/CuO is much larger than that of Al/ $\text{Cu}_2\text{O}$ . Therefore, it is beneficial to have more CuO and less  $\text{Cu}_2\text{O}$  in the CuOx if higher heat of reaction is desired for the Al/CuOx based EMs. To achieve this, normally longer thermal oxidation time is required. The reason is that when the Cu thin film is thermally oxidized in static air, Cu is first converted into  $\text{Cu}_2\text{O}$ . And then CuO is formed through a very slow oxidation of  $\text{Cu}_2\text{O}$  [23].

The thermite reactions of are characterized with DTA at a heating rate of 15 K/min. Figure 6a–d shows the DTA plots of the Al/CuOx based EMs, where the Cu films are oxidized in static air at 800  $^{\circ}\text{C}$  for 5 h, 360  $^{\circ}\text{C}$  for 5 h,



**Fig. 3** a, b SEM image and EDX pattern of the front side of the Al/CuO nEMs film. c, d SEM image and EDX pattern of the backside of the Al/CuO nEMs film

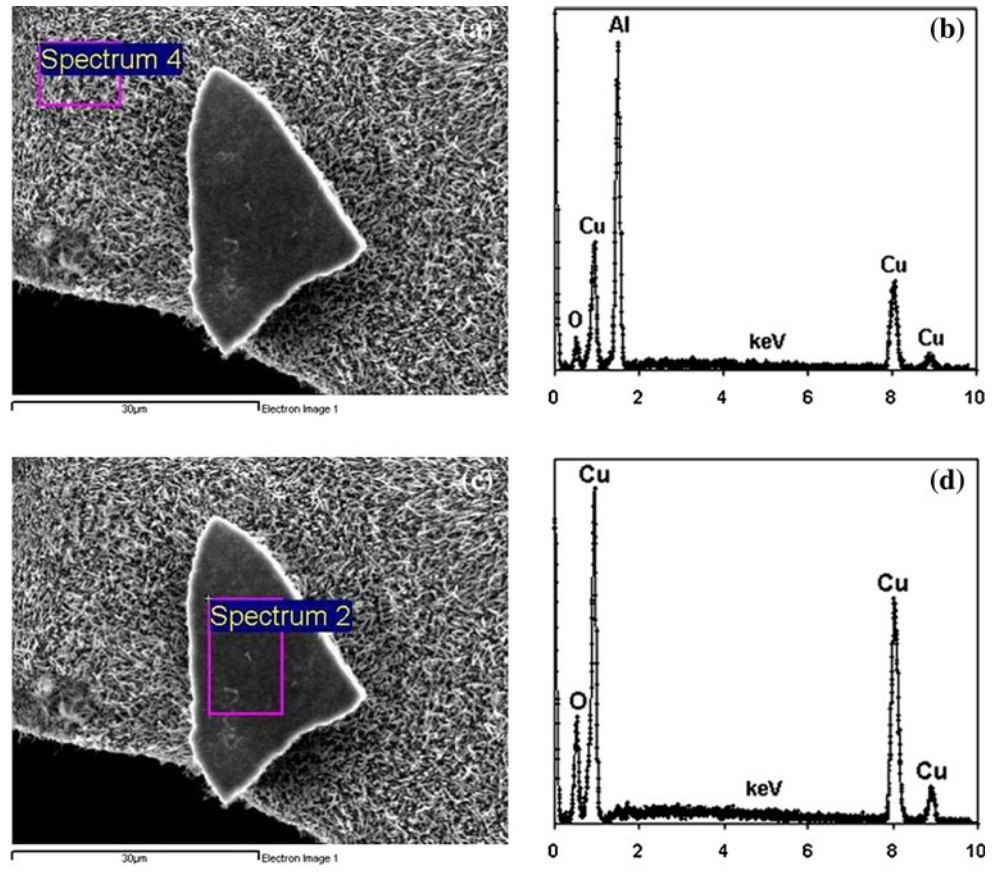


**Fig. 4** SEM image and elemental chemical map of the Al/CuO nEMs

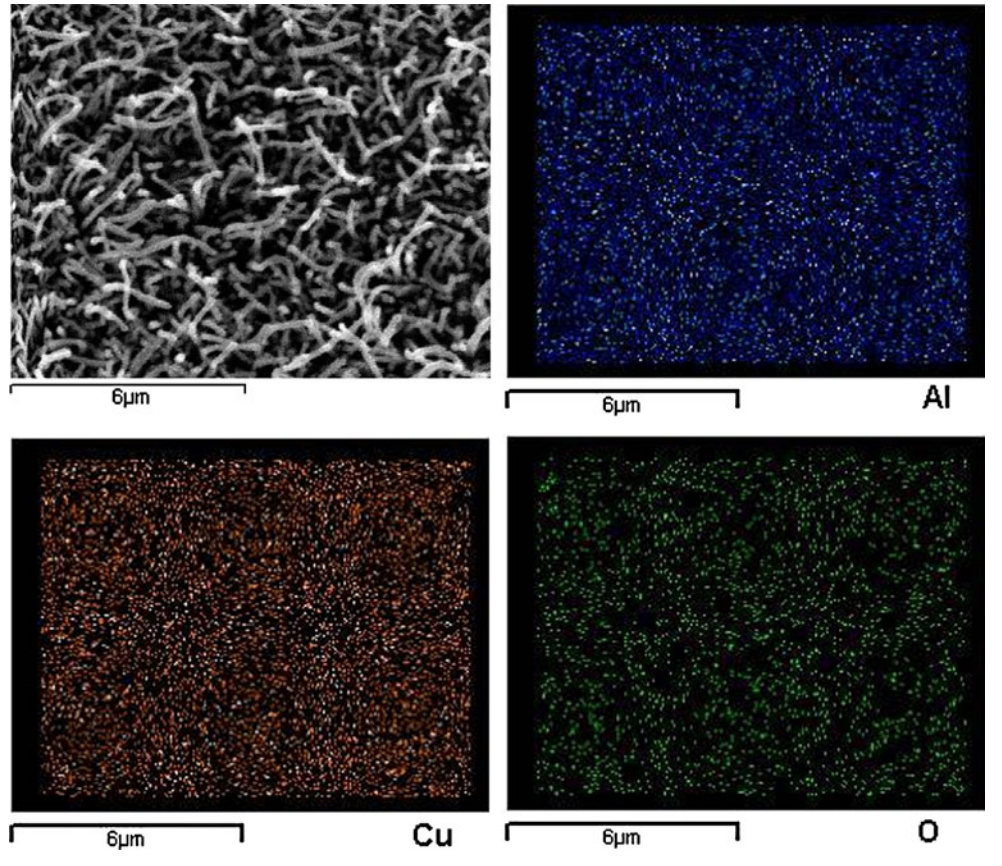


**Fig. 5** XRD patterns of the Al/CuOx based EMs, where the Cu films are oxidized in static air at: **a** 800 °C for 5 h, **b** 360 °C, 5 h, **c** 450 °C, 5 h, and **d** 450 °C, 14 h (the data in **c** are taken from Ref. [21])

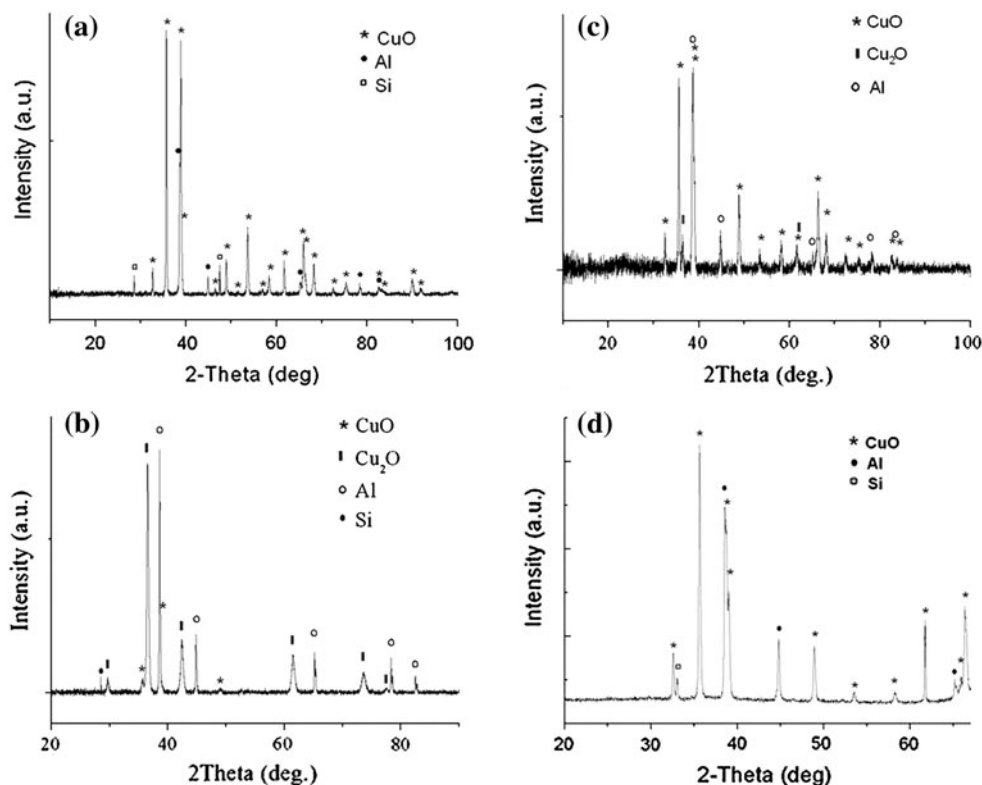


**Table 1** Heat of reaction and adiabatic temperatures for thermite reactions

	Heat of reaction ( $\Delta H$ ) (J/g)	Adiabatic temperature (K)
$3\text{CuO} + 2\text{Al} \rightarrow 3\text{Cu} + \text{Al}_2\text{O}_3$	4144	2846
$3\text{Cu}_2\text{O} + 2\text{Al} \rightarrow 6\text{Cu} + \text{Al}_2\text{O}_3$	2434	2846

450 °C for 5 h, and 450 °C for 14 h, respectively. And the sample masses for the DTA tests are 17.7, 12.8, 16.7, and 21.2 mg, respectively.

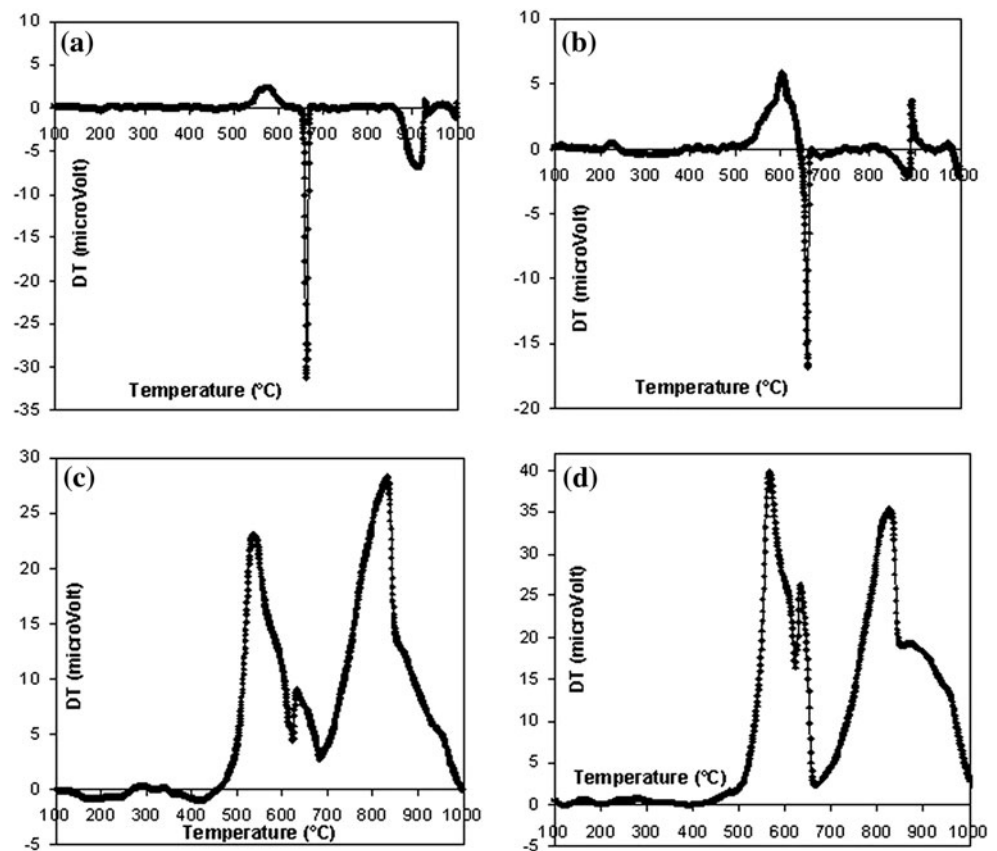
The thermite reactions of the Al/CuOx based EMs are also characterized with DSC at a heating rate of 5 K/min. Figure 7a–d shows the DSC plots of the Al/CuOx based EMs, where the Cu films are oxidized in static air at 800 °C for 5 h, 360 °C for 5 h, 450 °C for 5 h, and 450 °C for 14 h, respectively. And the sample masses for the DSC tests are 3.0, 4.6, 2.8, and 3.0 mg, respectively.

As shown in Fig. 6a, a very small exotherm (upwards) is observed with an onset temperature of about 520 °C, which is caused by the thermite reaction that remains limited only at the interface between the Al layer and the micro-sized CuO particles (see Figs. 1a, 2a). At around 660 °C, a sharp endothermic peak (downwards) is observed due to the melting of Al. Some endotherms and exotherms at high temperatures (>850 °C) are also observed which could be caused by the melting of Al–Cu intermetallics and/or Al–Cu oxides because  $\text{CuAlO}_2$  is found after DTA testing

at 1000 °C for the Al/CuO based nEM shown in Fig. 2c [21] and similar products are also found after DTA testing for CuOx/Al reactive multilayer foils [28]. In Fig. 6b, the first exothermic peak (peak area: ~620 J/g) with an onset temperature of about 520 °C is larger than the first exothermic peak (peak area: ~150 J/g) in Fig. 6a. This is because the nanostructures generated (nanowires and nanoparticles, see Fig. 1b) have a larger interfacial area with Al compared to the microstructures (see Fig. 1a). In Fig. 6c, the peak (peak area: ~1020 J/g) with an onset temperature of around 500 °C is around seven times larger than that in Fig. 6a. Indeed in this case the interfacial area between copper oxide and Al is very large because there are a great many nanowires (see Fig. 1c). At about 620 °C, there is an overlapping endothermic peak that is caused by the melting of Al. A second exotherm, with an onset temperature of about 670 °C, is also observed after the melting of Al. It is because of the reaction between the remaining Al and the microscale CuO/Cu<sub>2</sub>O thin films beneath the CuO nanowires. The DTA curve in Fig. 6d is very similar to that in Fig. 6c, which is as expected due to the similar structures of the Al/CuOx based EMs as can be seen in Fig. 1c, d and Fig. 2c, d.

In Fig. 7a, the first exothermic peak (upwards) with an onset temperature of about 500 °C, which corresponds to the first exothermic peak (upwards) in the DTA curve in Fig. 6a, is caused by the reaction at the interface between Al and the micro-sized copper oxide particles. The second

**Fig. 6** (Exothermic up) DTA plots of the Al/CuOx based EMs; the Cu films are oxidized in static air at: **a** 800 °C for 5 h, **b** 360 °C, 5 h, **c** 450 °C, 5 h, and **d** 450 °C, 14 h (the data in **c** are taken from Ref. [21])



endothermic peak ( $\sim 658$  °C, upwards) is caused by the melting of the remaining Al. The DSC curves in Fig. 7b–d are similar to that in Fig. 7a. Integration of the first exothermic peaks in the DSC curves in Fig. 7a–d gives the heat of the reactions for the different samples. These values are reported in Table 2. It is clear that the heat of reaction before Al melting is correlated with the amount of the CuO nanowires (see Fig. 1a–d and Fig. 2a–d). This further confirms the statement in Ref. [21] that the first exotherm in the DTA curve is caused by the thermite reaction between the CuO nanowires and nano-Al, which is based on the solid–solid diffusion mechanism. The specific structures (for example: defect structure or high surface area) of the CuO nanowires and Al nanoparticles provide higher surface energy that promotes the solid–solid diffusion process, which is probably the key factor contributing to the enhanced heat of reaction before Al melting.

#### Ignition study

To complement the SEM, EDX, XRD, DSC, and DTA data presented in “SEM characterization” to “DTA and DSC characterizations” sections, the ignition power, ignition delay, and ignition energy of the four kinds of Al/CuOx

based micro- and nano-EMs shown in Fig. 2 are investigated to compare their ignition properties. The ignition properties of the Al/CuOx nEM oxidized at 450 °C for 5 h shown in Fig. 2c has been studied in Ref. [22]. So ignition data in [22] are directly used here. Using the similar method, the ignition properties of the Al/CuOx based EMs shown in Fig. 2a, b, and d are further investigated in this study. Basically, copper thin films are deposited and patterned onto a Au/Pt/Cr microheater fabricated on a Pyrex-7740 glass substrate. Then the glass substrate is put into a high-temperature furnace to oxidize the copper thin film in static air at 800 °C for 5 h, 360 °C for 5 h, and 450 °C for 14 h, respectively. Unexpectedly, the glass substrate is greatly distorted and even partially melted after being heated at 800 °C for 5 h although its softening temperature is 820 °C as claimed by the supplier. As shown in Fig. 8a, the microheater on the glass substrate is also distorted. As a result, the Au/Pt/Cr microheater is damaged (resistance is infinite) and ignition testing cannot be done further for the Al/CuOx based EM shown in Fig. 2a. Here, we use ignition failure to describe this case. For the copper thin films oxidized at 360 °C for 5 h and 450 °C for 14 h, Al is deposited on them by thermal evaporation to form the Al/CuOx based EMs shown in Fig. 2b and d.



**Fig. 7** (Exothermic up) DSC plots of the Al/CuOx based EMs; the Cu films are oxidized in static air at: **a** 800 °C for 5 h, **b** 360 °C, 5 h, **c** 450 °C, 5 h, and **d** 450 °C, 14 h (the data in **c** are taken from Ref. [21])

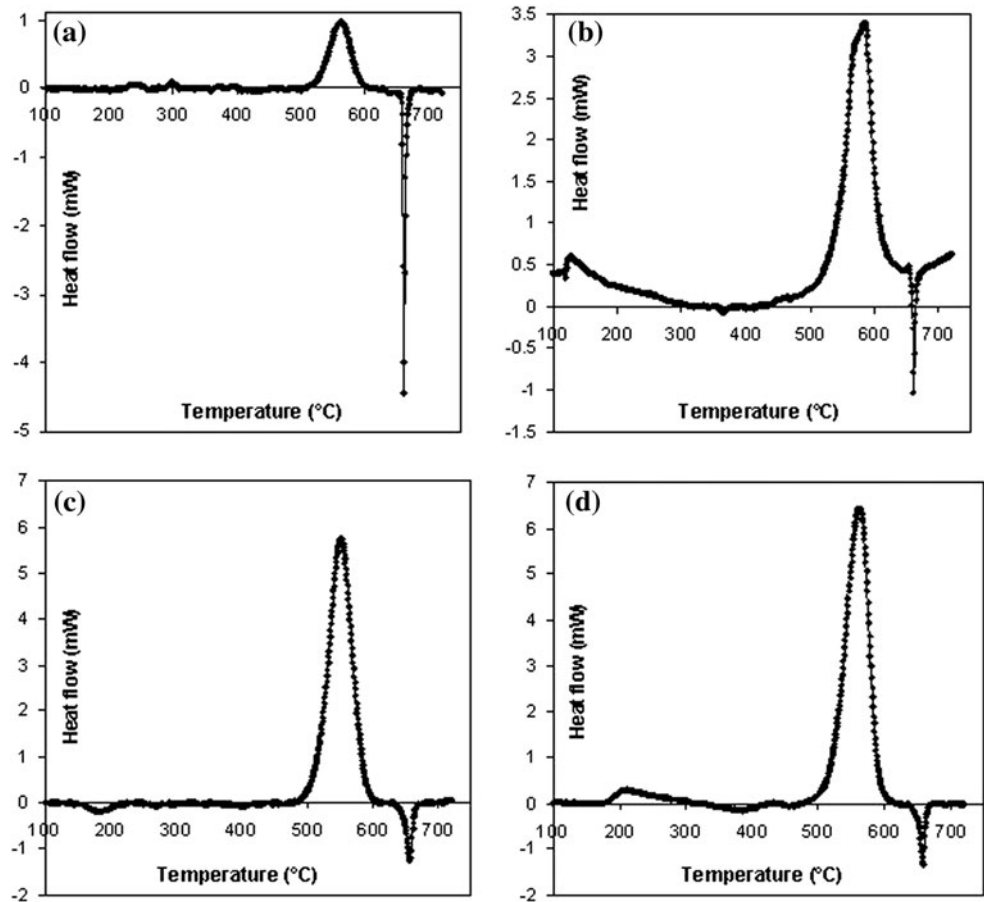


**Table 2** Comparison of the heat of reactions occurring before Al melting and the ignition properties

Synthesis conditions	800 °C, 5 h	360 °C, 5 h	450 °C, 5 h	450 °C, 14 h
Heat of reaction before Al melting (J/g)	150	620	1020	1140
Uncertainty (J/g)	±33.7	±23.5	±52.7	±50.6
Average ignition power (mW)	Failure	1.23	1.16	1.14
Average ignition delay (ms)	Failure	0.96	0.35	0.33
Average ignition energy (mJ)	Failure	1.18	0.41	0.38

To test the ignition properties, a voltage is input on the Au/Pt/Cr microheater with a current limitation of 0.35 A. The voltage and current variations with time are recorded simultaneously by a digital oscilloscope. Figure 8b–c shows the voltage and current variations with time for the ignition testing of the Al/CuOx based EMs, where Cu films are oxidized at 360 °C for 5 h, and 450 °C for 5 h, respectively, where the data used in Fig. 8c are taken from [22]. By comparing Fig. 8b and c, two main differences can be found. One is that a small

change (peak) is observed in the current curve at 0.2 ms in Fig. 8c, which is caused by the thermite reaction between nano-Al and CuO nanowires. The reaction heat causes the increase in the resistance of the microheater resulting in the decrease in the current. At 0.24 ms, the second major change (peak) is found in the current curve, which is due to the reactions between Al and CuO/Cu<sub>2</sub>O film beneath the CuO nanowires. However, only one major change (peak) is observed in the current curve in Fig. 8b. No small change (peak) before the major change in the current curve appears. This is because that the amount of CuO nanowires is very small when the copper film is oxidized at 360 °C for 5 h as shown in Fig. 1b. Consequently, the thermite reaction between the Al and nanowires is too weak to change the resistance of the microheater. The other difference is that the ignition delay in Fig. 8b is around three times longer than that in Fig. 8c. The possible reason is that the ignition (activation) temperature for the thermite reaction between Al and microscale CuO/Cu<sub>2</sub>O film (Fig. 8b) is higher than that for the reaction between Al and CuO nanowires (Fig. 8c). To reach a higher temperature in the microheater, more time is needed. There is no much difference in the ignition properties for the Al/CuOx



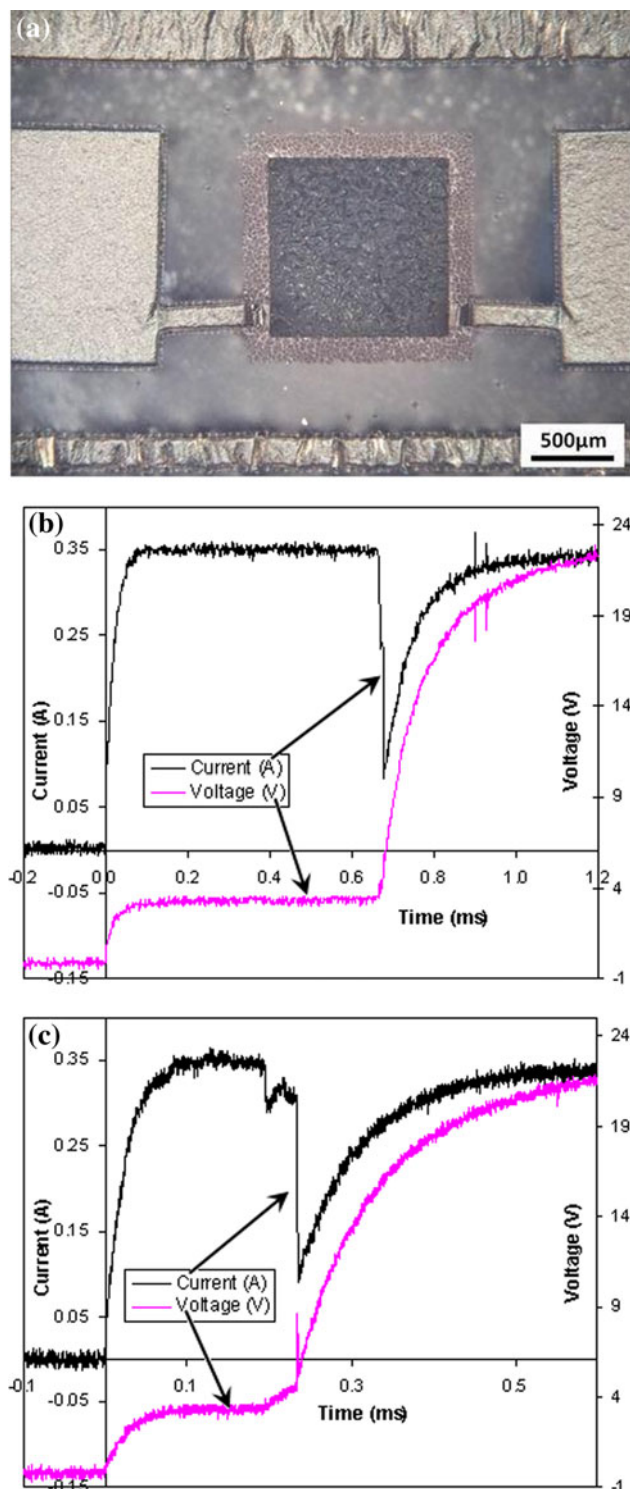


**Fig. 8** **a** Optical image of the Cu film on substrate after being heated at 800 °C for 5 h; **b**, **c** voltage and current variations with time for the ignition testing of the Al/CuOx based EMs, where Cu films are oxidized at 360 °C for 5 h and 450 °C for 5 h, respectively

based nEMs where the copper films are oxidized at 450 °C for 5 h and 450 °C for 14 h, respectively. The comparisons of the average ignition power, ignition

delay, and ignition energy for the four kinds of Al/CuOx based micro- and nano-EMs shown in Fig. 2 are listed in Table 2.

The different heat of reactions before Al melting and ignition properties of the four Al/CuOx based EMs shown in Table 2 prove that the nanostructures (CuO nanowires and nano-Al) make the EMs more reactive than microstructure based EMs. The different heat of reactions and ignition properties are also very useful for different applications. For instance, the Al/CuOx EMs synthesized at 800 °C for 5 h and 360 °C for 5 h are beneficial for the applications that require a low heat release at a low onset temperature (below Al melting temperature of 660 °C). The Al/CuOx EMs synthesized at 450 °C for 5 h and 450 °C for 14 h are useful for the applications that require a high heat release at a low onset temperature. They are also good for the applications that need short ignition delay and small ignition energy. While the Al/CuOx EMs synthesized at 360 °C for 5 h are useful for the applications that require longer ignition delay and higher ignition energy.

It also needs to mention that the exothermic reactions of the Al/CuO based nEMs are triggered from one point and then self-propagate throughout the  $1.2 \times 1.2 \text{ mm}^2$  area. This is because the thermite reactions of the Al/CuO based nEMs are extremely exothermic. Once the reaction is ignited, it generates sufficient heat to propagate the reaction through the remaining reactants. The self-propagating reactions also occur in reactive multilayer foils, which are typically sputter-deposited and have relatively flat easy to characterize interfaces [28–32]. The self-propagating exothermic reactions have promising applications in many areas such as self-propagating high-temperature synthesis (SHS), reaction initiation, fuses, microscale joining, soldering and brazing [28, 30–33].

## Conclusions

Al/CuOx based micro- and nano-EMs have been made by integrating Al with CuO microstructures and CuO nanostructures fabricated by thermal oxidation of Cu thin films deposited onto silicon substrates. The thermite reactions of the Al/CuOx based micro- and nano-EMs are investigated by DTA and DSC. It is found experimentally that the heat of reaction before Al melting (with an onset temperature of about 500 °C) is correlated with the amount of the CuO nanowires. This shows that the exothermic reaction between the CuO nanowires and Al can occur before Al melting. The experiments also indicate that the nanostructures (CuO nanowires and nano-Al) can help reduce the ignition delay and ignition energy of the Al/CuOx based EMs. One possible key factor contributing to the

enhanced thermite reactions and ignition properties of the CuO nanowires and Al based nEMs is that the higher surface energy associated with the CuO nanowires and the deposited nano-Al promotes the solid–solid diffusion process. The presented four kinds of Al/CuOx based micro- and nano-EMs in this study could meet the requirements for different applications that need a low or high heat release at a low onset temperature, small or high ignition delay and ignition energy.

## References

- Fried LE, Manaa MR, Pagoria PF, Simpson RL (2001) *Annu Rev Mater Res* 31:291
- Reddy B, Das K, Das S (2007) *J Mater Sci* 42:9366. doi: [10.1007/s10853-007-1827-z](https://doi.org/10.1007/s10853-007-1827-z)
- Rossi C, Zhang K, Esteve D, Alphonse P, Ching JYC, Tailhades P, Vahlas C (2007) *IEEE/ASME J Microelectromech Syst* 16(4):919
- Tillotson TM, Gash AE, Simpson RL, Hrubesh LW, Satcher JH Jr, Poco JF (2001) *J Non Cryst Solids* 285:338
- Menon L, Patibandla S, Ram KB, Shkuratov SI, Aurongzeb D, Holtz M, Berg J, Yun J, Temkin H (2004) *Appl Phys Lett* 84(23):4737
- Kim SH, Zachariah MR (2004) *Adv Mater* 16(20):1821
- Pantoya ML, Granier JJ (2005) *Propell Explos Pyrotech* 30(1):53
- Bockmon BS, Pantoya ML, Son SF, Asay BW, Mang JT (2005) *J Appl Phys* 98(6):064903
- Barbee TW, Simpson RL, Gash AE, Satcher JH (2005) U.S. Patent WO 2005 016850 A2
- Prakash A, McCormick AV, Zachariah MR (2005) *Nano Lett* 5(7):1357
- Pantoya ML, Granier JJ (2006) *J Therm Anal Calorim* 85(1):37
- Apperson S, Shende RV, Subramanian S, Tappmeyer D, Gangopadhyay S, Chen Z, Gangopadhyay K, Redner P, Nicholich S, Kapoor D (2007) *Appl Phys Lett* 91:243109
- Walter KC, Pesiri DR, Wilson DE (2007) *J Propuls Power* 23(4):645
- Puszynski JA, Bulian CJ, Swiatkiewicz JJ (2007) *J Propuls Power* 23(4):698
- Sanders VE, Asay BW, Foley TJ, Tappan BC, Pacheco AN, Son SF (2007) *J Propuls Power* 23(4):707
- Son SF, Asay BW, Foley TJ, Yetter RA, Wu MH, Risha GA (2007) *J Propuls Power* 23(4):715
- Dutro GM, Yetter RA, Risha GA, Son SF (2009) *Proc Combust Inst* 32:1921
- Martirosyan KS, Wang L, Vicent A, Luss D (2009) *Nanotechnology* 20:405609
- Currano LJ, Churaman WA (2009) *IEEE/ASME J Microelectromech Syst* 18(4):799
- Ohkura Y, Liua SY, Raoa PM, Zheng X (2011) *Proc Combust Inst* 33(2):1909
- Zhang K, Rossi C, Tenailleau C, Alphonse P, Rodriguez GAA (2007) *Appl Phys Lett* 91(11):113117
- Zhang K, Rossi C, Petrantoni M, Mauran N (2008) *IEEE/ASME J Microelectromech Syst* 17(4):832
- Jiang X, Herricks T, Xia Y (2002) *Nano Lett* 2(12):1333
- Liu Y, Liao L, Li J, Pan C (2007) *J Phys Chem C* 111:5050
- Park YW, Seong NJ, Jung HJ, Chanda A, Yoon SG (2010) *J Electrochem Soc* 157:K119
- Xu CH, Woo CH, Shi SQ (2004) *Chem Phys Lett* 399:62
- Zhang K, Rossi C, Tenailleau C, Alphonse P, Ching JYC (2007) *Nanotechnology* 18(27):275607
- Blobaum KJ, Reiss ME, Lawrence JMP, Weihs TP (2003) *J Appl Phys* 94(5):2915
- Gavens AJ, Van Heerden D, Mann AB, Reiss ME, Weihs TP (2000) *J Appl Phys* 87(3):1255
- Wang J, Besnoin E, Knio OM, Weihs TP (2005) *J Appl Phys* 97:114307
- Trenkle JC, Weihs TP, Hufnagel TC (2008) *Scr Mater* 58(4):315
- Rogachev AS (2008) *Russ Chem Rev* 77(1):21
- <http://www.indium.com/nanofoil/>